Spectral density reconstruction with Chebyshev polynomials

Joanna E. Sobczyk [1,*] and Alessandro Roggero [2,3,4,†]

[1]*Institut für Kernphysik and PRISMA+ Cluster of Excellence, Johannes Gutenberg-Universität, 55128 Mainz, Germany*
[2]*Physics Department, University of Trento, Via Sommarive 14, I-38123 Trento, Italy*
[3]*INFN-TIFPA Trento Institute of Fundamental Physics and Applications, Trento, Italy*
[4]*InQubator for Quantum Simulation (IQuS), Department of Physics, University of Washington, Seattle, Washington 98195, USA*

Accurate calculations of the spectral density in a strongly correlated quantum many-body system are of fundamental importance to study its dynamics in the linear response regime. Typical examples are the calculation of inclusive and semiexclusive scattering cross sections in atomic nuclei and transport properties of nuclear and neutron star matter. Integral transform techniques play an important role in accessing the spectral density in a variety of nuclear systems. However, their accuracy is in practice limited by the need to perform a numerical inversion which is often ill-conditioned. In the present work we extend a recently proposed quantum algorithm which circumvents this problem. We show how to perform controllable reconstructions of the spectral density over a finite energy resolution with rigorous error estimates. An appropriate expansion in Chebyshev polynomials allows for efficient simulations also on classical computers. We apply our idea to obtain the local density of states for graphene in a magnetic field as a proof of principle. This paves the way for future applications in nuclear and condensed matter physics.

I. INTRODUCTION

A major challenge in nuclear many-body theory is the accurate prediction of scattering cross sections in low-energy reactions involving both atomic nuclei and infinite nuclear matter. For *ab initio* approaches with a strong connection to the underlying theory of QCD it is fundamental to be able to control the approximation errors in both the employed interactions and the adopted many-body method. With the help of an effective field theory approach the first of this sources of uncertainty has begun to be put on a firmer ground [1–6], and theoretical error estimates coming from the modeling of nuclear interactions are now an integral part of the work of nuclear theorists [7–10]. Using similar tools great efforts are being pursued by the nuclear theory community to understand the systematic errors introduced by the approximate many-body techniques used to solve the nuclear ground states [11,12]. Benchmark calculations for ground-state properties of few-body nuclei have also been performed (see, e.g., [13]), but a more complete understanding of the various sources of systematic errors in predictions of nuclear dynamics for larger systems is hindered by the incredible computational complexity of the problem.

A very powerful approach to study dynamical properties in medium-mass systems and infinite matter is the adoption of integral transform techniques which map the local density of states into more manageable integrated quantities, a typical example being sum rules of the nuclear response which

describe moments of the density of states and can be expressed directly as ground-state expectation values [14,15]. This important map between real-time observables and ground-state expectation values can be achieved more generally by employing integral transforms with various kernels followed by a numerical inversion of the resulting integral transform to recover the response function in the frequency domain. The choice of integral kernel is typically dictated by the possibility of evaluating the ensuing integral transform with a powerful many-body technique. Two of the most popular examples are the Lorentz integral transform (LIT) widely used in conjunction with diagonalization techniques [16,17] and, more recently, the coupled cluster method (LIT-CC) [18–20] and the Laplace transform applied with Monte Carlo methods due to its relationship with imaginary-time correlation functions [21–23]. A crucial component of these approaches consists in inverting the integral transform, a process that for the Laplace transform can be seen as analytical continuation from imaginary-time to the real time axis [24]. In general this procedure when applied to invert an integral transform obtained by numerical methods is ill-posed, in the sense that small errors in the input response can give rise to arbitrarily large high-frequency noise in the reconstructed real frequency response [25,26]. A variety of approximate inversion techniques that introduce, more or less explicitly, additional smoothing to reduce these high-frequency oscillations have been proposed in the past [27–31]. These can be very successful in situations where the dominant structure of the response function is simple and known beforehand, such as for the quasielastic peak in medium energy scattering [23,32], but the introduced systematic errors are no longer sufficiently under control to trust predictions with unexpected

---
*jsobczyk@uni-mainz.de
†a.roggerog@unitn.it

features thus severely limiting explorations of the nuclear dynamics in challenging regimes where little experimental information is available to guide the inversion.

At this point it is important to mention that some observables connected with integrated properties of the response, like, e.g., the electric dipole polarizability of nuclei [33] or the impurity contribution to the thermal conductivity in the outer crust of neutron stars [34], can be obtained directly from the integral transform thus allowing one to avoid the inversion step. Moreover, the severity of the induced systematic errors strongly depends on the properties of the integral kernel that defines the integral transform, a feature recognized early on and one of the inspirations for introducing the LIT in nuclear physics [16,35] as well as generalizations of the Laplace transform [36,37]. One of the salient features of an ideal integral transform kernel is the ability to set a resolution scale which then allows for an effective coarse graining of the frequency space signal; e.g., for the LIT this is controlled by the kernel width. This intuition led recently to the introduction of quantum algorithms to reliably estimate both inclusive and exclusive scattering cross sections through an appropriate integral transform of the spectral density using simulations performed with quantum computers [38–40] (see also [41–43] for similar approaches and [44,45] for recent reviews).

In this work we extend the results of Ref. [39] to show how to reconstruct, with controllable errors, a general response function in frequency space from integral transforms expressed on a basis of Chebyshev polynomials thus completely avoiding the use of uncontrollable numerical inversion procedures. The use of Chebyshev polynomials for this task is reminiscent of the kernel polynomial method (KPM) [46] introduced in the context of condensed matter physics and especially popular in conjunction with a matrix product representation (see, e.g., [47–49]).

The paper is organized as follows. In the next section we briefly describe the approach introduced in Ref. [39] for the calculation of the spectral density discussing differences and similarities with KPM. The method's accuracy and its dependence on the particular choice of integral kernel are discussed in Sec. III, where we also compare it directly with the more standard KPM approach. In Sec. IV we introduce a construction for coarse graining the spectral density in a way that allows for a direct control of the approximation error and study a simple benchmark to show its efficacy. We present also an application of our method to obtain predictions of the local density of states for graphene in a magnetic field. Finally, in Sec. V we conclude and discuss the potential benefit of our proposal when used in conjunction with classical many-body techniques like matrix product states and coupled cluster theory.

II. FORMALISM

Following the presentation in Ref. [39] we start by introducing the local density of states (or dynamical response function) defined as

$$S(\omega) = \frac{\langle \Psi_0 | \hat{O} \delta(\hat{H} - \omega) \hat{O} | \Psi_0 \rangle}{\langle \Psi_0 | \hat{O}^2 | \Psi_0 \rangle}, \quad (1)$$

where $|\Psi_0\rangle$ is the ground state, $\hat{O}$ is an (Hermitian) excitation operator describing the scattering vertex, and $\hat{H}$ is the nuclear Hamiltonian. Note that with this definition the density of states is normalized as $\int d\omega S(\omega) = 1$. For finite systems the Hamiltonian spectrum is discrete by construction, but here we consider ω as a continuous variable by employing the Dirac δ function as

$$S(\omega) = \sum_n \frac{|\langle \Psi_0 | \hat{O} | \phi_n \rangle|^2}{\langle \Psi_0 | \hat{O}^2 | \Psi_0 \rangle} \delta(E_n - \omega) = \sum_n s_n \delta(E_n - \omega), \quad (2)$$

with $|\phi_n\rangle$ energy eigenstates with eigenvalues E_n. Furthermore, we will assume that the Hamiltonian has been normalized so that the entire spectrum $\{E_n\}$ is contained in the interval $[-1, 1]$. As explained in the introduction, the main focus of this work will be an integral transform $\Phi(\nu)$ of the response function defined through an integral kernel $K(\nu, \omega)$ as

$$\Phi(\nu) = \int_{-\infty}^{\infty} d\omega K(\nu, \omega) S(\omega). \quad (3)$$

In this work we will focus on translationally invariant integral kernels that depend only on the absolute value of the energy difference $K(\nu, \omega) \equiv K(|\omega - \nu|)$, but the results described here can be easily extended to the general case. For ease of derivation the limits of integration extend to $\pm\infty$, with the understanding that $S(\omega) = 0$ for $|\omega| > 1$. In order to simplify the notation we will avoid to specify these limits when there is no ambiguity. We are in general interested in observables that can be expressed as energy integrals of the local density of state $S(\omega)$ as

$$Q(S, f) = \int d\omega S(\omega) f(\omega) \quad (4)$$

with a bounded function $f(\omega)$ defining the specific observable under consideration. Using the integral transform Φ introduced in Eq. (3) we can define the quantity

$$
\begin{aligned}
Q(\Phi, f) &= \int d\nu \Phi(\nu) f(\nu) \\
&= \int d\nu \int d\omega K(|\omega - \nu|) S(\omega) f(\nu) \\
&= \int d\omega \left[\int d\nu K(|\omega - \nu|) f(\nu) \right] S(\omega) \\
&= \int d\omega \widetilde{f}(\omega) S(\omega) = Q(S, \widetilde{f}). \quad (5)
\end{aligned}
$$

Our goal is to determine the conditions for which the latter is a good approximation to the original observable

$$|Q(\Phi, f) - Q(S, f)| = |Q(S, \widetilde{f}) - Q(S, f)| \leqslant \epsilon, \quad (6)$$

with bounded error $\epsilon > 0$. For this purpose, it is convenient to define integral kernels to be Σ-*accurate* with *resolution* Λ (see also Ref. [39]) if the following holds:

$$\inf_{\omega_0 \in [-1,1]} \int_{\omega_0 - \Lambda}^{\omega_0 + \Lambda} d\nu K(\nu, \omega_0) \geqslant 1 - \Sigma. \quad (7)$$

As shown in Ref. [39], for this class of kernels we have

$$\epsilon \leqslant f_{max}^{\Lambda} + 2\Sigma \sup_{\omega \in [-1,1]} |f(\omega)|, \quad (8)$$

with f_{max}^{Λ} the modulus of continuity given by

$$f_{max}^{\Lambda} = \sup_{\omega \in [-1,1]} \sup_{x \in [-\Lambda,\Lambda]} |f(\omega + x) - f(\omega)|. \qquad (9)$$

In this work we will consider two types of translationally invariant integral kernels with an energy resolution controlled by an external parameter λ:

(1) The Lorentzian kernel describing the Lorentz integral transform (LIT) from Ref. [16]

$$K^{(L)}(\nu, \omega; \lambda) = \frac{1}{\pi \lambda} \frac{\lambda^2}{(\omega - \nu)^2 + \lambda^2} \qquad (10)$$

(2) The Gaussian kernel giving the Gaussian integral transform (GIT) from Ref. [39]

$$K^{(G)}(\nu, \omega; \lambda) = \frac{1}{\sqrt{2\pi}\lambda} \exp\left[-\frac{(\omega - \nu)^2}{2\lambda^2}\right]. \qquad (11)$$

In order to evaluate the integral transform $\Phi(\nu)$ using a suitable many-body method, we will consider an expansion of these kernels into a complete basis of orthogonal polynomials $\{T_k(\omega)\}$ as

$$K(\nu, \omega; \lambda) = \sum_k^{\infty} c_k(\nu; \lambda) T_k(\omega), \qquad (12)$$

with real coefficients $c_k(\nu; \lambda)$ depending both on the location in energy ν and the kernel resolution λ. With this representation we can now express the integral transform as a linear combination

$$\Phi(\nu; \lambda) = \int d\omega K(\nu, \omega; \lambda) S(\omega) = \sum_k^{\infty} c_k(\nu; \lambda) m_k \qquad (13)$$

with generalized moments defined as

$$m_k = \int d\omega T_k(\omega) S(\omega) = \frac{\langle \Psi_0 | \hat{O} T_k(\hat{H}) \hat{O} | \Psi_0 \rangle}{\langle \Psi_0 | \hat{O}^2 | \Psi_0 \rangle} \qquad (14)$$

and independent on the specific integral kernel employed in the construction. This property is particularly advantageous since, once the moments $\{m_k\}$ are computed with the many-body method of choice, it allows one to consider a variety of integral transforms in post-processing.

In practice, only a limited number N of moments will be available with a finite computational effort. Their calculation—in the case of many-body systems governed by complicated dynamics—is very challenging and requires powerful supercomputer due to high time and memory consumption. This cost can, however, be substantially lower than what would be required to calculate the full energy spectrum. In the latter case, for an $M \times M$ Hamiltonian matrix, the cost is $O(M^3)$ but for the moment calculation only $O(NM^2)$. Using instead quantum computing, as originally proposed in Ref. [39], the cost can be made to scale as $O(N\text{polylog}(M))$ for large classes of interacting Hamiltonians (e.g., Hamiltonian operators in second quantization describing two- and three-body interactions). We will then consider approximations to integral transforms obtained by a finite truncation of the series expansion

$$\Phi_N(\nu; \lambda) = \sum_k^{N} c_k(\nu; \lambda) m_k, \qquad (15)$$

leading to a finite approximation accuracy

$$\sup_{\nu \in [-1,1]} |\Phi(\nu; \lambda) - \Phi_N(\nu; \lambda)| \leqslant \beta, \qquad (16)$$

with constant $\beta > 0$. Ideal kernels, like the Gaussian, have a fast (i.e., exponential) convergence of β with the number of terms N. Note that this is not the approximation error of $S(\omega)$ by Eq. (15) but the approximation error of $\Phi(\nu, \lambda)$. The former cannot be known without additional information about S, while the latter can be controlled independently and depends only on the required resolution and the choice of kernel. The choice of the polynomial basis $\{T_k\}$ influences this convergence rate. In this work we use the Chebyshev polynomials of the first kind due to their quick convergence for smooth functions, and we will refer to our method as CheET (Chebyshev expansion of integral transforms). An explicit derivation of the coefficients $c_k(\nu; \lambda)$ for both the Lorentzian and Gaussian kernels can be found in Appendix A.

A. Evaluation of Chebyshev moments

Chebyshev polynomials of the first kind are defined in the interval $[-1, 1]$ as $T_k(\omega) = \cos[k \arccos(\omega)]$. They follow a recursive relation

$$T_0(x) = 1; \quad T_{-1}(x) = T_1(x) = x,$$
$$T_{n+1}(x) = 2x T_n(x) - T_{n-1}(x). \qquad (17)$$

The moments of the expansion m_k from Eq. (14) can be retrieved using the relation

$$|\Psi_1\rangle \equiv \hat{O}|\Psi_0\rangle, \quad |\Psi_n\rangle = \hat{H}|\Psi_{n-1}\rangle$$
$$m_0 = \langle \Psi_1 | \Psi_1 \rangle, \quad m_1 = \langle \Psi_1 | \Psi_2 \rangle \equiv \langle \Psi_2 | \Psi_1 \rangle$$
$$m_{n+1} = 2\langle \Psi_1 | \Psi_{n+1} \rangle - m_{n-1} \equiv 2\langle \Psi_{n+1} | \Psi_1 \rangle - m_{n-1}, \quad (18)$$

which is particularly suited to combine with the many-body methods for which it is possible to iterate the action of the Hamiltonian, $\hat{H}|\Psi_n\rangle$. From the point of view of the numerical applications, a similar iteration has to be performed in the Lanczos procedure [46]. Here, however, no orthogonality restoration is needed at each step. Consequently, at the nth step only a single $|\Psi_n\rangle$ state has to be saved from the previous iterations. This makes the procedure faster and less memory consuming.

As has been mentioned, in our considerations we assume that the Hamiltonian is normalized. In practical applications the range of the Hamiltonian spectrum can be obtained, e.g., via the Lanczos algorithm and then rescaled so that $[E_{min}, E_{max}] \rightarrow [-1, 1]$.

B. Comparison with KPM

The KPM, described in detail in Ref. [46], can be understood as a specific approximation of Eq. (12) for which

$$K_{\text{KPM}}(\nu, \omega; \lambda) = \sum_k^{\infty} g_k(\lambda) \frac{T_k(\nu)}{\pi \sqrt{1 - \nu^2}} T_k(\omega), \qquad (19)$$

where the ν dependence of the c_k coefficients is approximated by a single k-degree polynomial $T_k(\nu)$ times a fixed weight factor $1/\sqrt{1 - \nu^2}$. The coefficients g_k are chosen in such a way that $\Phi(\omega) \xrightarrow[N \to \infty]{} S(\omega)$ and to reduce Gibbs oscillations.

A variety of g_k were proposed in the past, designed to speed up the convergance rate depending on the properties of the signal $S(\omega)$. Among them are the Jackson and Lorentz kernels defined as

$$g_k^{\text{Jackson}} = \frac{1}{N+1}\left[(N-k+1)\cos\frac{\pi k}{N+1}\right.$$
$$\left. + \sin\frac{\pi k}{N+1}\cot\frac{\pi}{N+1}\right],$$
$$g_k^{\text{Lorentz}} = \sinh[\kappa(1-k/N)]/\sinh(\kappa), \quad (20)$$

which aim at approximating the Gaussian and Lorentzian shape of the kernel. It is important to notice that the KPM coefficients g_k do not depend on the resolution λ, while they are a function of the total number of moments N. (The parameter κ in the case of g_k^{Lorentz} is introduced to mimic indirectly the λ dependence.) In other words, λ and N dependencies become entangled in a nontrivial way. This complicates the error analysis, as we have a different kernel for every choice of N and ultimately leads to less flexibility in balancing the computational cost with the target accuracy. Although the KPM is a powerful tool which proved useful in many applications, it does not allow one to control either the resolution λ with which we probe the spectrum or the errors depending on the number of used moments.

III. ANALYSIS OF POINTWISE CONVERGENCE

To appreciate the differences between the CheET and KPM approaches, let us first consider a continuous signal $S(\omega)$ being a single Gaussian of width $\Gamma = 0.1$ or $\Gamma = 0.01$ centered at $\eta = 0.3$. We have checked that our conclusions hold if the signal has a Lorentzian shape or when it is composed of more than one peak (in this case the convergence pattern depends on the narrowest peak in the spectrum). Since the KPM method was primarily developed for the signal reconstruction, we will analyze the pointwise convergence. However, the main advantage of the CheET method—the error bound—cannot be appreciated in this case. For the comparison to be meaningful, within the CheET we will use kernels of the width $\lambda \ll \Gamma$.

Before discussing the results of this comparisons, it is important to point out that the optimal (at least asymptotically) choice for performing an approximation of a smooth signal $S(\omega)$ over the interval $[-1, 1]$ would be to consider directly the Chebyshev expansion of $S(\omega)$ without the use of any smoothing kernel. The reason for this is a well-known result by Jackson (see Ref. [50,51]) stating that, if $P_N(\omega)$ is the approximation obtained by keeping the first N terms in the Chebyshev expansion of $S(\omega)$, then

$$\sup_{\omega\in[-1,1]} |S(\omega) - P_N(\omega)| \leqslant C_N 6 S_{max}^{1/N}, \quad (21)$$

with a Lebesgue constant $C_N \leqslant [2 + (2/\pi)\log(N+1)]$ (see Ref. [52]) and $S_{max}^{1/N}$ the modulus of continuity of $S(\omega)$ over an interval of size $1/N$ [see definition in Eq. (9) above]. This classic result shows that a bare Chebyshev expansion for an analytic response $S(\omega)$, like the Gaussian used for the examples in this section, will converge superexponentially in the order N of the expansion. In order to estimate the error, however, we need to be able to estimate $S_{max}^{1/N}$ or at least a

reasonably tight upper bound for it. In the applications of interest for our study we have access only to the first N moments of $S(\omega)$, and this, alone, does not provide enough information to obtain an error estimate from Eq. (21) directly. Furthermore, without prior information about the behavior of the moments of $S(\omega)$ for $n > N$, we also cannot place a rigorous error bound on the truncation error of the expansion. The adoption of a smoothing kernel $K(\nu, \omega)$ enables us instead to consider an approximation $\Phi(\omega, \lambda)$ to $S(\omega)$ with controllable smoothing properties [obtained from the condition in Eq. (7)] for which we can compute an upper bound β on the truncation error which converges exponentially in the order N and which does not require any knowledge about the target response $S(\omega)$. This can be obtained, even without knowing the value of moments m_k for $k > N$, using the following bound:

$$|\Phi(\nu; \lambda) - \Phi_N(\nu; \lambda)| = \left|\sum_{k=N+1}^{\infty} c_k(\nu; \lambda)m_k\right|$$
$$\leqslant \sum_{k=N+1}^{\infty} |c_k(\nu; \lambda)|, \quad (22)$$

which, when maximized over ν, gives in turn an upper bound on the truncation error β defined in Eq. (16).

Due to the necessary smoothing, we cannot place directly a bound on the approximation error of $S(\omega)$ by $\Phi(\omega, \lambda)$, but for the applications described in Sec. IV where we are interested in observables of the type shown in Eq. (5) this is not needed. In the latter case, a useful, and rigorous, error estimate can be obtained from the properties of the function f alone. The purpose of this section is to show that, empirically, the approximation error is also very small and approaches the optimal result quickly for sufficiently small regularization width λ. This is not the case for the procedure used in KPM where the impact of regularization is orders of magnitude more severe.

Let us first look at the reconstruction within each of the considered methods in the case of the signal width $\Gamma = 0.1$. In Fig. 1 we show the results only for the Jackson and Gaussian kernels, since the behavior of the kernels within each method (Jackson/Lorentz or Gauss/Lorentz) is qualitatively the same. The first visible distinction between the KPM and the CheET with $\lambda = 0.01$ results is the fact that the Gibbs oscillation is suppressed for the KPM approach. Still, the CheET Gaussian is visibly better converged at much lower number of moments (already for $N = 60$).

To get a more quantitative insight into the convergence pattern, in Fig. 2 we show the pointwise convergence as a function of used moments (and λ for the CheET), for the broad signal $\Gamma = 0.1$ and the narrow $\Gamma = 0.01$,

$$\vartheta = \max_{\omega\in[-1,1]} |S(\omega) - \Phi(\omega)|, \quad (23)$$

where Φ is an integral transform of the signal S, as in Eq. (3). As a reference we plot a result with no kernel, which, as explained above, converges faster than any other smoothing method. We use $\kappa = 3$ for the Lorentz KPM [see Eq. (20)]. The CheET curves follow a characteristic pattern: after the initial steep-slope convergence, they reach a plateau. Further addition of moments would improve the kernel reconstruction (and thus diminish the truncation error); however, this does
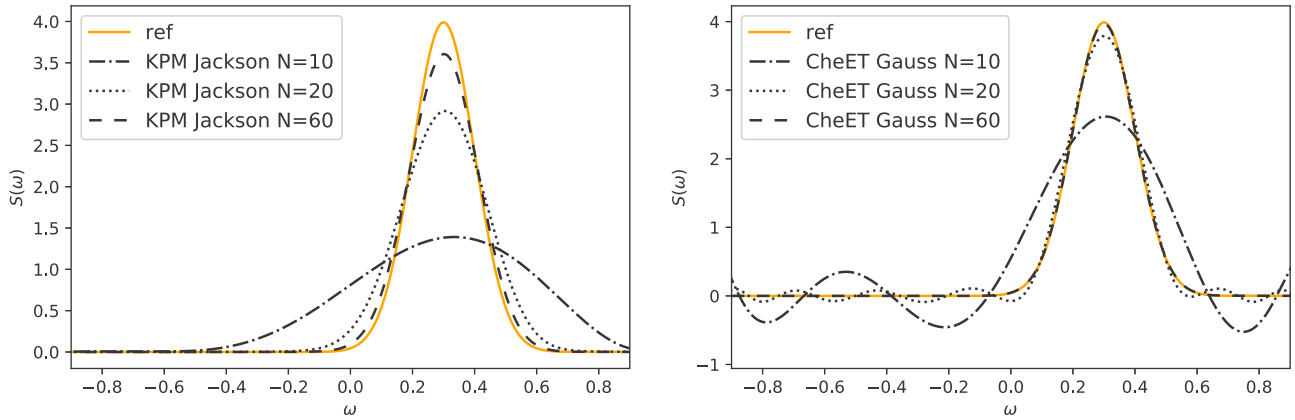
FIG. 1. Reconstruction of a Gaussian signal $S(\omega)$ of a width $\Gamma = 0.1$ centered at $\eta = 0.3$. In the case of the CheET method, $\lambda = 0.01$ is used

not affect the quality of signal approximation. The exact number of moments needed to reach the plateau depends on the signal itself, in particular on the signal's resolution Γ. This can be seen when comparing both panels of Fig. 2. Using kernels of the same resolution λ, not only a higher number of moments is needed for smaller Γ, but also the plateau is reached with different accuracy. For $\lambda = 0.001$, the CheET Gaussian reaches an accuracy $\sim e^{-8}(e^{-1})$ for $\Gamma = 0.1(0.01)$.

A direct comparison of CheET with the Lorentzian and Gaussian kernels with the same width λ clearly shows that in the latter case the convergence is orders of magnitude better. In order to obtain results of a similar precision, we would need to use a Lorentzian of a much smaller width. This consequently requires a larger number of moments if we are to control the truncation error.

In the case of the pointwise error considered here, neither KPM nor CheET is able to give a full theoretical uncertainty estimation. Using the KPM method has an advantage that with the increasing number of moments N, we converge to the original signal $\Phi_{\text{KPM}}^N(\omega) \xrightarrow{N \to \infty} S(\omega)$. However, the pace of convergence or the approximation error is unknown. From our observations, the CheET rate of convergence (before reaching a plateau) is much faster than KPM. Although for a given resolution λ the CheET method reaches a plateau, in the limit

$N \to \infty$ the CheET predictions can also converge to the original signal. In order to achieve this we should progressively reduce the resolution λ of the kernel with the increasing number of moments. We may do so by appropriately scaling $\lambda(N)$, e.g., by keeping fixed the truncation error at a satisfactory low value. This behavior can be actually observed in Fig. 2 when we compare various CheET results with the reference curve without any smoothing kernel. They initially follow the same steep-slope convergence pattern, until the CheET curves reach the plateau.

For the CheET, we are still able to provide an estimate for the truncation error β as a function of number of moments used for the reconstruction of the kernel. In Fig. 3 we show the bound obtained using the approximation in Eq. (22) for eight values of λ (see Appendix B for closed-form expressions for these). As expected, the Gaussian kernel performs better than the Lorentzian. For the truncation error to be at the order of 0.1 and $\lambda = 0.01$ one needs $N \approx 900$ moments. To go an order of magnitude further to $\lambda = 0.001$, the number of moments increases correspondingly to $N \approx 10\,000$. When comparing these numbers with Fig. 2, we realize that the plateau is reached much faster, even below $N = 100$. This discrepancy is likely coming from the use of the bound in Eq. (22), which erases structural information from the moments and therefore
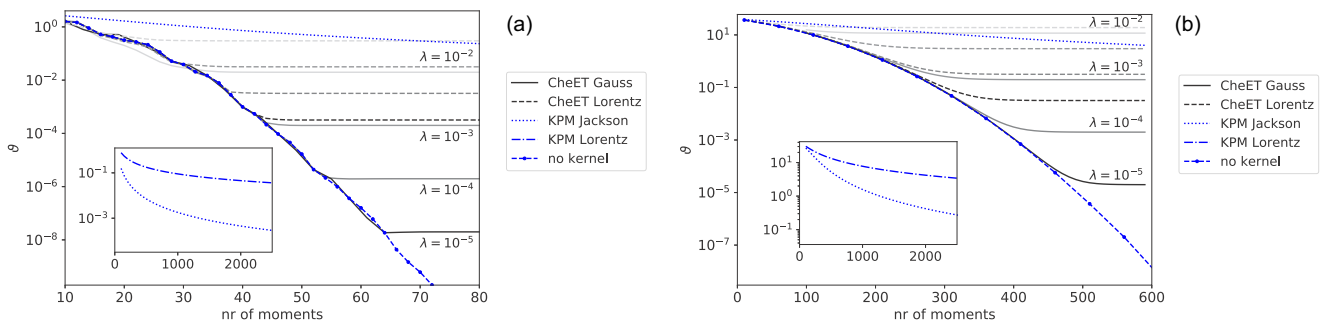

FIG. 2. Comparison of the pointwise convergence of CheET and KPM methods for a Gaussian signal of width $\Gamma = 0.1(0.01)$ on the left (right) panel. The measure of convergence ϑ is defined in Eq. (23). Solid lines correspond to CheET method with the Gaussian kernel of λ resolution as labeled. The results for CheET Lorentzian kernel (dashed lines) have λ corresponding to the Gaussian CheET. The dashed line with point markers shows the convergence pattern when no kernel is used. The inset shows the behavior of KPM (both Jackson and Lorentz) for a much larger number of moments.
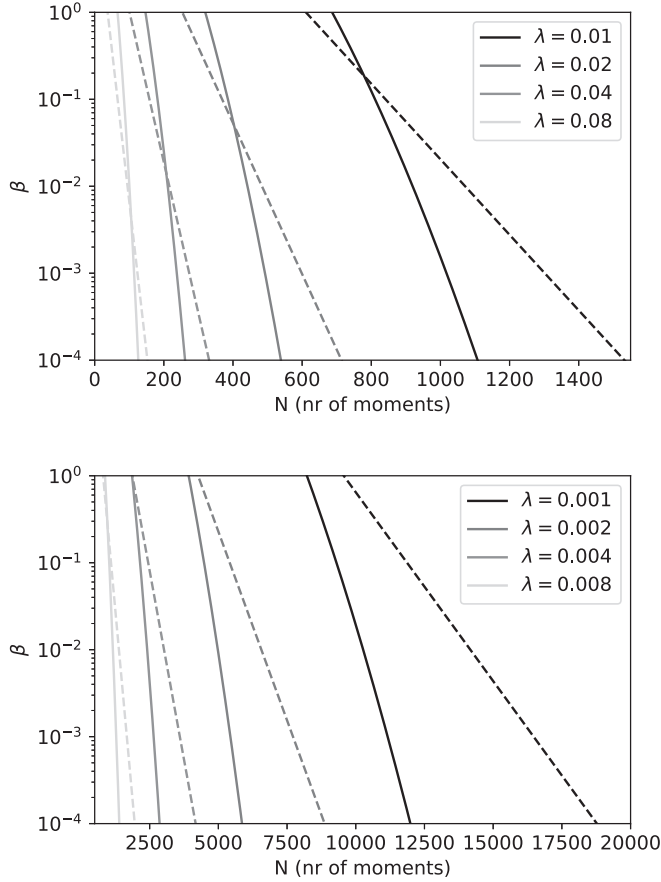
FIG. 3. Truncation error as a function of number of moments. Solid (dashed) line corresponds to CheET Gaussian (Lorentzian) for eight resolutions λ.
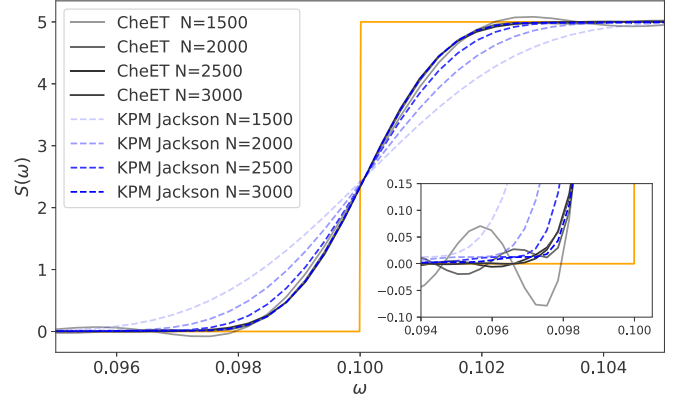

FIG. 4. Reconstruction of a step function using KPM with Jackson kernel and CheET Gaussian for four values of $N = 1500, 2000, 2500, 3000$. In case of CheET the kernel width $\lambda = 0.001$ was chosen.

The pointwise convergence in this case is not a meaningful measure, since in the vicinity of the discontinuity $\omega = 0.1$ we have $\exists_{\Delta\omega} S(\omega + \Delta\omega) - \Phi(\omega + \Delta\omega) \approx 2.5$. Nevertheless, we depict in Fig. 4 this region to see the convergence behavior of KPM Jackson and CheET Gaussian methods. For the CheET we choose the resolution $\lambda = 0.001$, and for the number of moments between $N = 1500$–3000 we observe nearly overlapping curves, which—for lower N—suffer from the Gibbs oscillations (as shown in the inset). This again manifests that we control the reconstruction through λ, not through the number of moments (their number has to be sufficient only to control the truncation error β). For the KPM the increasing number of moments corresponds heuristically to smaller λ. The flexibility afforded by the CheET strategy allows to obtain results qualitatively similar to KPM with $N = 3000$ using only $N \approx 2500$ moments.

IV. DIRECT APPROXIMATION OF THE SPECTRAL DENSITY USING HISTOGRAMS

The results shown in the previous section are useful to gain insights into the possible benefits of using different kernel functions to study the local spectral density. For a more realistic case when the target response is not known, however, it will not be possible to compute directly the pointwise error from Eq. (23), and a different, computable, error metric is needed. We achieve this by explicitly introducing a target energy resolution scale Δ and using the properties enjoyed by Σ-*accurate* with *resolution* Λ integral kernels to bound the error on a suitably coarse-grained energy distribution. For this purpose, we introduce an energy histogram as a frequency observable like Eq. (5) by defining the following window function

$$f(\omega, \eta; \Delta) = \begin{cases} 0 & |\eta - \omega| > \Delta \\ 1 & \text{otherwise} \end{cases}. \tag{25}$$

The histogram of the frequency signal $S(\omega)$, with associated bin width equal to 2Δ, is found by integrating over the spectrum. Explicitly, the value of the histogram centered at η is

assumes the truncation is for a worse-case scenario signal of width $\approx \lambda$ instead.

Let us come back to a remark made in Sec. II B. While in the case of KPM (at least for the Jackson kernel), the only free parameter of the signal reconstruction is N, the number of moments used in the reconstruction, the CheET method introduces explicitly a smoothing scale λ which corresponds to the regularization parameters used for the standard inversion techniques. When the signal has structures of a higher resolution, we are not able to resolve them. At first sight it might seem to be a drawback. However, λ gives directly the scale at which we can rely on the signal reconstruction. This is lacking in the KPM, for which in the asymptotic regime we might never see a uniform convergence of errors. Moreover, in practical applications one has only a limited number of moments available and would like to reconstruct the signal controlling the approximation. This can be done within CheET. The resolution scale can be set depending on N to keep the truncation errors sufficiently low.

To further illustrate the differences between both approaches, we present yet another comparison, this time taking as a signal a step function normalized to 1,

$$S(\omega) = \begin{cases} 5 & \text{if } \omega \in [0.1, 0.3] \\ 0 & \text{otherwise} \end{cases}. \tag{24}$$

given by

$$h(\eta; \Delta) = \int_{-1}^{1} d\omega S(\omega) f(\omega, \eta; \Delta) = \int_{\eta-\Delta}^{\eta+\Delta} d\omega S(\omega). \quad (26)$$

We now define an approximate histogram by taking the convolution of the window function in Eq. (25) with an integral kernel with resolution Λ:

$$\widetilde{f}^{\Lambda}(\omega, \eta; \Delta) = \int_{-1}^{1} d\nu K(\nu, \omega; \Lambda) f(\nu, \eta; \Delta)$$

$$= \int_{\eta-\Delta}^{\eta+\Delta} d\nu K(\nu, \omega; \Lambda). \quad (27)$$

The resulting approximate histogram can be written as

$$\widetilde{h}^{\Lambda}(\eta; \Delta) = \int_{-1}^{1} d\omega \widetilde{f}^{\Lambda}(\omega, \eta; \Delta) S(\omega)$$

$$= \int_{-1}^{1} d\omega \int_{\eta-\Delta}^{\eta+\Delta} d\nu K(\nu, \omega; \Lambda) S(\omega). \quad (28)$$

Finally, we will further approximate $\widetilde{h}^{\Lambda}(\eta; \Delta)$ as a Chebyshev expansion truncated to order N introducing an error bounded by

$$\sup_{\eta \in [-1,1]} |\widetilde{h}^{\Lambda}(\eta; \Delta) - \widetilde{h}_N^{\Lambda}(\eta; \Delta)| \leqslant 2\Delta \beta. \quad (29)$$

Using these quantities we can then approximate the histogram with bin size 2Δ at η using the following pair of bounds:

$$\widetilde{h}_N^{\Lambda}(\eta; \Delta - \Lambda) - \Sigma - 2\beta(\Delta - \Lambda) \leqslant h(\eta, \Delta),$$

$$h(\eta, \Delta) \leqslant \widetilde{h}_N^{\Lambda}(\eta; \Delta + \Lambda) + \Sigma + 2\beta(\Delta + \Lambda). \quad (30)$$

The derivation of Eq. (30) can be found in Appendix C, the truncation errors $\beta^{(G,L)}$ for the Gaussian and Lorentzian are given in Eqs. (B5) and (B22) in Appendix B. Last, the tails Σ [see the definition in Eq. (7)] for the Lorentz and Gaussian kernels are bounded by

$$\Sigma^{(L)} \leqslant \frac{2\lambda}{\pi\Lambda}, \quad \Sigma^{(G)} \leqslant \exp\left(-\frac{\Lambda^2}{2\lambda^2}\right). \quad (31)$$

The approximated histogram bin of Eq. (28) can be expressed in terms of Chebyshev moments expansion

$$\widetilde{h}^{\Lambda}(\eta; \Delta) = \int_{\eta-\Delta}^{\eta+\Delta} d\nu \sum_k c_k(\nu, \lambda) m_k$$

$$= \sum_k d_k(\eta - \Delta, \eta + \Delta, \lambda) m_k, \quad (32)$$

with d_k coefficients which can be obtained analytically from the c_k and are given in Eq. (A21) for the Gaussian kernel. Through this procedure we do not introduce any further numerical error and the calculation cost of c_k and d_k coefficients is of the same order. On the other hand, using the KPM to calculate a histogram would more troublesome, since in this case using the kernel of Eq. (19) one gets

$$\widetilde{h}^{\Lambda}(\eta; \Delta) = \int_{\eta-\Delta}^{\eta+\Delta} d\nu \sum_k g_k(\lambda) \frac{T_k(\nu)}{\pi\sqrt{1-\nu^2}} m_k. \quad (33)$$

The integral has no analytical closed form, therefore its calculation has to be done numerically which is computationally more expensive.

A. Synthetic data

We will consider an example of the signal reconstruction of both a discrete and continuous spectrum, in terms of a histogram. To generate the synthetic data we will use a function

$$g(x) = \sqrt{x - 0.8} \exp\left(-\frac{x}{0.35}\right), \quad (34)$$

which is qualitatively similar to nuclear responses in the quasielastic regime.

1. Discrete signal

In this case we generate the synthetic data by mimicking a many-body calculation for which the spectrum has a discrete form as in Eq. (2). For this study, the spectrum is generated as a uniform random distribution of 500 delta peaks with strengths taken from Eq. (34) (the total strength is normalized to 1) in a range $(-0.8, 1)$.

2. Continuous signal

We generated a continuous function using directly Eq. (34), with the total strength normalized to 1.

In our example we take the width of histogram bins to be $2\Delta = 0.2$. For the CheET method we set a desired kernel resolution to be $\Lambda = 0.01$. This is driven by the following observation. Looking at Eq. (30), we see that when the kernel is accurate enough (Σ is small) and we keep the truncation error β low (i.e., we use a sufficient number of moments), the uncertainty is driven by $(\tilde{h}_{\Delta+\Lambda} - \tilde{h}_{\Delta-\Lambda})$. Therefore we expect the error to be roughly proportional to Λ/Δ. For the chosen values of Δ and Λ, we keep it at the order of $\approx 10\%$.

Having set Λ, we should choose λ, so that the tails of the distributions Σ [see Eq. (31)] are small enough. Finally, knowing λ, the truncation error β as a function of number of moments N can be estimated. In Fig. 5 we show the total truncation error $2\beta(\Delta + \Lambda)$ and the tail bound Σ in relation to (λ, N) for a chosen $\Delta = 0.1$ and $\Lambda = 0.01$, for both the Gaussian and Lorentz kernels. The horizontal lines correspond to $\Sigma^{(L,G)}$. In the right panel where $\lambda = 0.001$, $\Sigma^{(G)}$ is already negligibly small and not visible. A compromise between the number of used moments N and the desired accuracy λ has to be found. From the central panel of Fig. 5, we conclude that $\lambda = 0.0025$ is good enough to quench $\Sigma^{(G)}$, while keeping the number of moments $N = 4000$. For this value of N, and for the Lorentzian kernel the truncation error is smaller than $\Sigma^{(L)}$.

The results for both discrete and continuous signals for this setup are shown in Fig. 6. All the results, both KPM and CheET, correspond to $\tilde{h}_N^{\Lambda}(\eta; \Delta)$, i.e., truncated expansion of Eq. (28) with the same number of moments $N = 4000$. All four predictions give similar results which stay in agreement with the reference signal. However, the error estimation, given in Eq. (30), is not available for the KPM approach. The large errors for CheET Lorentz come mostly from $\Sigma^{(L)} \propto \lambda/\Lambda$. They have been divided by factor 2 in Fig. 6, to fit them in
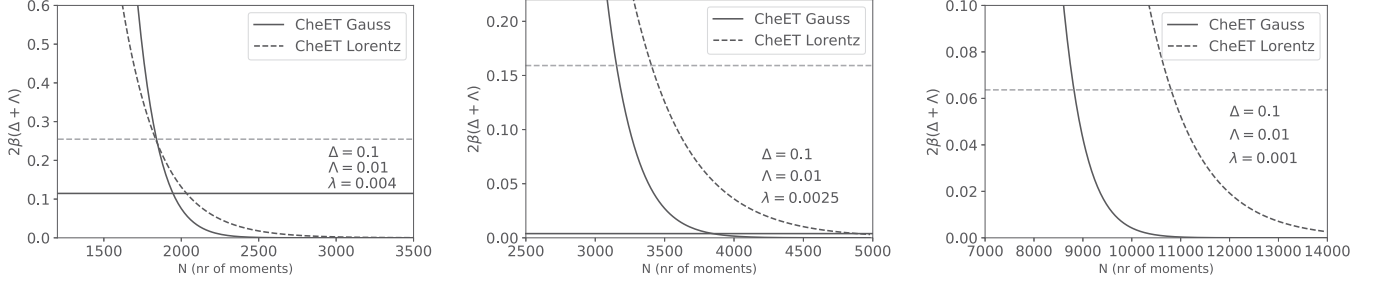
FIG. 5. Truncation error as a function of number of moments, for a histogram bin $2\Delta = 0.2$. Kernel resolution is $\Lambda = 0.01$, using $\lambda = 0.004, 0.0025, 0.001$ are shown, respectively, on the left, central, and right panels. The dashed curves correspond to the Lorentzian kernel. The horizontal dashed and solid lines in each plot correspond to $\Sigma^{(L)}$ and $\Sigma^{(G)}$ (the tail bound). In the right panel $\Sigma^{(G)}$ is already orders of magnitude smaller and not visible at this scale.

the plots. They could be diminished by improving the precision λ, which would consequently require a larger number of moments. From the right panel of Fig. 5 we see that diminishing this error by factor 2.5 would require $\lambda = 0.001$ and so over $N = 10\,000$ moments. At the same time, the CheET Gaussian gives much better uncertainty estimation. The tail bound $\Sigma^{(G)}$ and truncation error β are negligible in this case, and the uncertainty is driven by the difference $\tilde{h}^{\Lambda}(\eta, \Delta + \Lambda) - \tilde{h}^{\Lambda}(\eta, \Delta - \Lambda)$.

B. Graphene in a magnetic field

As a proof of principle, we apply our method to obtain the local density of states (LDOS) for graphene in a magnetic field. We choose a single layer of graphene with the circular shape and radius of 30 nm in a magnetic field of 20 T. We use the Pybinding [53] Python library to retrieve the Chebyshev moments.

Within the KPM or the CheET method we would be able to get the spectrum of single peaks (with a given broadening), resolving the excitations in the vicinity of $E = 0$ which correspond to Landau levels. However, the density of states grows with energy so that the reconstruction of higher-lying states requires an increasing number of Chebyshev moments. Instead, we create a histogram to show the LDOS in the whole range of energies $(-8.45, 8.45)$ eV. For our simulation we set the histogram width 0.4 eV, $\Lambda = 0.05$ eV, and $\lambda = 0.015$ eV. The results shown in Fig. 7 were performed using $N = 5000$ moments. This number of moments corresponds to the broadening of 5 meV in the Jackson KPM method, which allows us to distinguish the first five Landau levels, up to the energy ± 0.3 eV. We plot as a reference $f(E) \propto E^{3/2}$, to show that the distribution is in good approximation (up to $E \approx 2$ eV) related to the positions of Landau states, with $E_n \propto \sqrt{n}$, since $\int \sqrt{n}\,dn = n^{3/2}$. The error bars in Fig. 7 are mostly driven
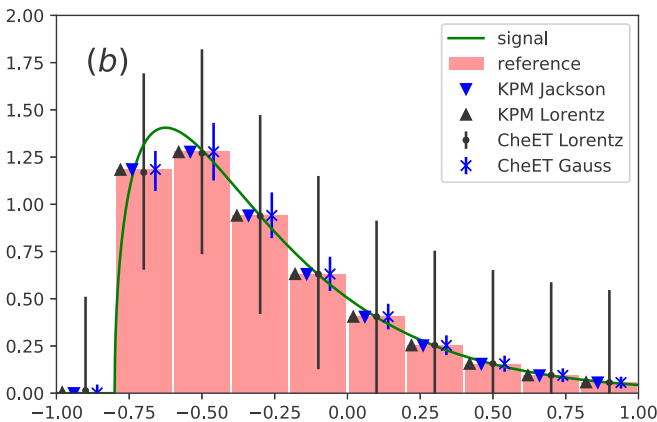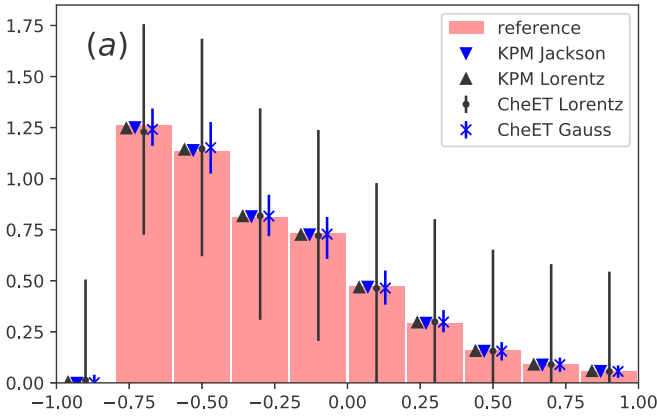

FIG. 6. Signal reconstruction for a discrete case (upper panel) and a continuous case (lower panel). In both cases the CheET Lorentz error bars were rescaled by factor 0.5.
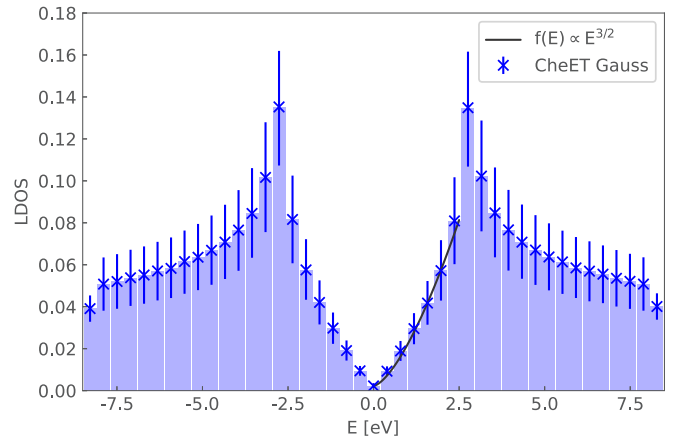

FIG. 7. Local density of states of the monolayer graphene in a magnetic field of 20 T reconstructed using CheET method with Gaussian kernel.

by $\widetilde{h}_N^\Lambda(\eta; \Delta + \Lambda) - \widetilde{h}_N^\Lambda(\eta; \Delta - \Lambda)$ [see Eq. (30)]. In this case the spectrum is uniform, therefore we suspect the errors $\approx \Lambda/\Delta = 0.05/0.2 = 25\%$, which indeed is the case. This uncertainty could be quenched by diminishing Λ, which would require a larger number of Chebyshev moments.

V. SUMMARY AND CONCLUSIONS

Predicting the dynamical response of strongly coupled many-body systems is a problem of central importance in nuclear physics since most of the experimental information comes from scattering cross sections. A quantitative understanding of many-body dynamics is also crucial in cold atoms experiments and quantum chemistry. In the linear response regime, the scattering cross section is related to the local spectral density, a notoriously difficult observable to evaluate in *ab initio* methods. In this work we have presented a method for the reconstruction of the spectral density starting from an expansion in terms of Chebyshev polynomials using earlier results discussed in the context of quantum algorithms [39]. This idea is similar in spirit to both the kernel polynomial method (popular in condensed matter) and to the Lorentz integral transform method (employed in nuclear physics). Importantly, the approach presented here allows for a systematic control of the errors in the reconstruction, a key ingredient which is in general not easily achievable in both of the above mentioned techniques.

Our results are an important step which will directly allow us to perform a full *ab initio* calculation of dynamical response functions in many-body systems. In particular, they pave the way to extend the LIT-CC calculations [18–20] to compute observables for which the inversion procedure may be numerically unstable. The approach presented in this work can also be beneficial as an extension of KPM in applications using tensor networks [48,49] and the new error bounds on the histogram discretization will provide additional guidance for the design of quantum algorithms for the estimation of the spectral density [39,43].

In the future work we plan to address two further issues. First of all, the error estimates derived here are not necessarily tight (especially the truncation error for the Gaussian kernel in Appendix B 2) and it will be beneficial to improve the accuracy of the bounds. Second, the present method does not allow to estimate another major source of systematic bias in these calculations: the presence of an artificially discrete spectrum coming from the need to carry the many-body simulation in a finite basis. This is taken care of in the LIT framework by a careful choice of the energy resolution of the kernel. Performing a benchmark of these strategies in solvable models will be an important step forward that we will address in the future.

APPENDIX A: CHEBYSHEV MOMENTS FOR INTEGRAL KERNELS

In this Appendix we provide a complete derivation of the Chebyshev moments c_k for the Lorentzian and Gaussian kernels defined in Eqs. (10) and (11),

$$K^{(G,L)}(\nu, \omega; \lambda) = \sum_{k=0}^{\infty} c_k(\nu, \lambda) T_k(\omega), \qquad (A1)$$

used in the main text.

1. Moments for Lorentzian kernel

Following Ref. [54] the Chebyshev expansion of the Lorentzian can be written as

$$K^{(L)}(\nu, \omega; \lambda) = \frac{1}{\pi} \sum_{k=0}^{\infty} (2 - \delta_{k,0}) \mathcal{R}[D_\lambda(\nu) Z_\lambda(\nu)^k] T_k(\omega) \qquad (A2)$$

where $\mathcal{R}[z]$ is the real part of z and the two functions are defined as

$$D_\lambda(\nu)^{-1} = \sqrt{1 - (\nu + i\lambda)^2},$$
$$Z_\lambda(\nu) = (\nu + i\lambda) - iD_\lambda(\nu)^{-1}. \qquad (A3)$$

If we consider the situation where $(\nu^2 + \lambda^2) < 1$ we can express the second factor explicitly as

$$Z_\lambda(\nu) = -i \exp\left[i \arcsin(\nu + i\lambda)\right] = -ie^{-\lambda}e^{i\nu}. \qquad (A4)$$

If we also decompose the first factor in polar coordinates $D_\lambda(\nu)^{-1} = \rho e^{i\theta}$ we can write compactly the coefficient in the Chebyshev expansion as

$$c_k^{(L)}(\nu; \lambda) = \mathcal{R}[D_\lambda(\nu) Z_\lambda(\nu)^k]$$
$$= \rho^{-1} e^{-k\lambda} \cos\left[k\left(\nu - \frac{\pi}{2}\right) - \theta\right]. \qquad (A5)$$

2. Moments for Gaussian kernel

We start the discussion by first recalling the Chebyshev expansion of a Gaussian function

$$\frac{1}{\sqrt{2\pi}\lambda} e^{-\frac{\omega^2}{2\lambda^2}} = \sum_{k=0}^{\infty} a_k(\lambda) T_k(\omega), \qquad (A6)$$

where the moments $a_k(\lambda)$ are given explicitly as

$$a_n = \begin{cases} \frac{\gamma_n}{\sqrt{2\pi}\lambda} i^{\frac{n}{2}} \exp\left(-\frac{1}{4\lambda^2}\right) J_{n/2}\left(\frac{i}{4\lambda^2}\right) & \text{for even } n \\ 0 & \text{for odd } n \end{cases} \qquad (A7)$$

with $\gamma_n = 2 - \delta_{n,0}$ and J_n, the Bessel function of order n.

Using this expansion, the Gaussian kernel can be expressed as

$$K^{(G)}(\nu, \omega; \lambda) = \sum_{k=0}^{\infty} a_k\left(\frac{\lambda}{2}\right) T_k\left(\frac{\nu - \omega}{2}\right), \quad \text{(A8)}$$

in terms of Chebyshev polynomials depending on both variables ν and ω. Our goal is instead to find a decomposition in terms of polynomials in ω of the form of Eq. (A1)

The procedure proposed in Ref. [39] to obtain the moments $c_k(\nu, \lambda)$ proceeds as follows: we first perform the expansion

$$T_k\left(\frac{\nu - \omega}{2}\right) = \sum_{m=0}^{\infty} b_m^k(\nu) T_m(\omega), \quad \text{(A9)}$$

with expansion coefficients given by

$$b_m^k(\nu) = \frac{\gamma_m}{\pi} \int_{-1}^{1} \frac{d\omega}{\sqrt{1 - \omega^2}} T_k\left(\frac{\nu - \omega}{2}\right) T_m(\omega). \quad \text{(A10)}$$

Apart from the weight factor $1/\sqrt{1 - \omega^2}$, the integrand is a polynomial in ω of maximum degree $D = k + m$. This in turn implies that, if we can perform the integration exactly using Gauss-Chebyshev quadrature as

$$b_m^k(\nu) = \frac{\gamma_m}{\pi} \sum_{i=1}^{L} w_i T_k\left(\frac{\nu - \omega_i}{2}\right) T_m(\omega_i) \quad \text{(A11)}$$

with weights $w_i = \frac{\pi}{L}$ and Chebyshev nodes

$$\omega_i = \cos\left(\pi \frac{2i - 1}{2L}\right), \quad \text{(A12)}$$

provided we choose $L > (D + 1)/2$. In the following we will take $L = L_{m,k} = \lceil (m + k + 1)/2 \rceil$.

Now, by realizing that, for any choice of ν, the function $T_k[(\nu - \omega)/2]$ is a polynomial of order k in ω, the sum in Eq. (A9) can be truncated at order $m \geq k$ without incurring in an approximation error. This implies that we can take, for a given k, the truncation in Eq. (A11) as

$$L = L_{k,k} = \left\lceil \frac{2k + 1}{2} \right\rceil = k + 1. \quad \text{(A13)}$$

Suppose now that we approximate the Gaussian kernel with a truncated sum of the form

$$K^{(G),N}(\nu, \omega; \lambda) = \sum_{k=0}^{N} a_k\left(\frac{\lambda}{2}\right) T_k\left(\frac{\nu - \omega}{2}\right)$$

$$= \sum_{k=0}^{N} \sum_{m=0}^{\infty} a_k\left(\frac{\lambda}{2}\right) b_m^k(\nu) T_m(\omega), \quad \text{(A14)}$$

with a corresponding truncation error $\beta_N^{(G)}$ derived in Ref. [39] and discussed in more detail in the next Appendix. In the original derivation in Ref. [39] the expansion in m was truncated at $m = N \geq k$ resulting in

$$K^{(G),N}(\nu, \omega; \lambda) = \sum_{k=0}^{N} \sum_{m=0}^{N} a_k\left(\frac{\lambda}{2}\right) b_m^k(\nu) T_m(\omega)$$

$$= \sum_{m=0}^{N} \left[\sum_{k=0}^{N} a_k\left(\frac{\lambda}{2}\right) b_m^k(\nu) \right] T_m(\omega)$$

$$= \sum_{m=0}^{N} \widetilde{c}_m^{[N]}(\nu, \lambda) T_m(\omega), \quad \text{(A15)}$$

with expansion coefficients given explicitly as

$$\widetilde{c}_m^{[N]}(\nu, \lambda) = \sum_{k=0}^{N} \sum_{i=1}^{L_{k,k}} \frac{\gamma_m}{L_{k,k}} a_k\left(\frac{\lambda}{2}\right) T_k\left(\frac{\nu - \omega_i^k}{2}\right) T_m(\omega_i^k), \quad \text{(A16)}$$

with Chebyshev nodes ω_i^k depending explicitly on k due to the corresponding k dependence of the number of terms $L_{k,k}$. As in Ref. [39] this can be removed by performing a further simplification by choosing $L_{k,k} = N + 1$ independent on k. As the discussion on the Gaussian quadrature formula provided above shows, this does not introduce further errors and results in a modest $O(N)$ increase in number of summands. The final expression for the expansion coefficients is then[1]

$$\widetilde{c}_m^{[N]}(\nu, \lambda) = \frac{\gamma_m}{N + 1} \sum_{k=0}^{N} \sum_{i=1}^{N+1} a_k\left(\frac{\lambda}{2}\right) T_k\left(\frac{\nu - \widetilde{\omega}_i}{2}\right) T_m(\widetilde{\omega}_i), \quad \text{(A17)}$$

where we have defined the k-independent nodes

$$\widetilde{\omega}_i = \cos\left[\pi \frac{2i - 1}{2(N + 1)} \right]. \quad \text{(A18)}$$

We will call the scheme presented so far *method 1*. It has one main disadvantage with respect to the construction for the Lorentz kernel above: evaluation of the kernel (or equivalently the integral transform) at different frequencies ν incurs in a cubic cost with the number of terms N whereas for the Lorentz kernel this cost is only linear in N. Another drawback of the present construction is that the coefficients $\widetilde{c}_m(\nu, \lambda)$ in the kernel expansion of Eq. (A15) and provided explicitly in Eq. (A17) are not the same as the $c_k(\nu, \lambda)$ coefficients obtained from a direct univariate expansion of the kernel in the ω frequency as in Eq. (A1). As we will see below this might result in a worse truncation error, at fixed N, than one could obtain if the latter expansion coefficients were known analytically (as in the case of the Lorentzian).

To address both of these problems, here we also consider a second approach that directly estimates the "exact" coefficients

$$c_k(\nu, \lambda) = \frac{\gamma_k}{\pi} \int_{-1}^{1} \frac{d\omega}{\sqrt{1 - \omega^2}} K^{(G)}(\nu, \omega; \lambda) T_k(\omega) \quad \text{(A19)}$$

by approximating the integral with a Gauss-Chebyshev quadrature using a large number of nodes $M > N$ for a target truncation level N:

$$c_k^{[N,M]}(\nu, \lambda) = \sum_{m=1}^{M} \frac{\gamma_k}{M} K^{(G)}(\nu, \omega_m; \lambda) T_k(\omega_m) \quad \text{(A20)}$$

with $\omega_m = \cos(\pi \frac{2m-1}{2M})$ the Chebyshev nodes as above. This construction, *method 2* has the main advantage of resulting in a faster evaluation of the kernel and integral transform.

─────────

[1]We note two typos in Ref. [39] with $(N + 1)$ being indicated as N and the numerator in Eq. (A18) being quoted to be (effectively) $2i + 1$ instead of $2i - 1$. These do not affect any of the results discussed there but are important for a correct implementation of the expansion coefficients.
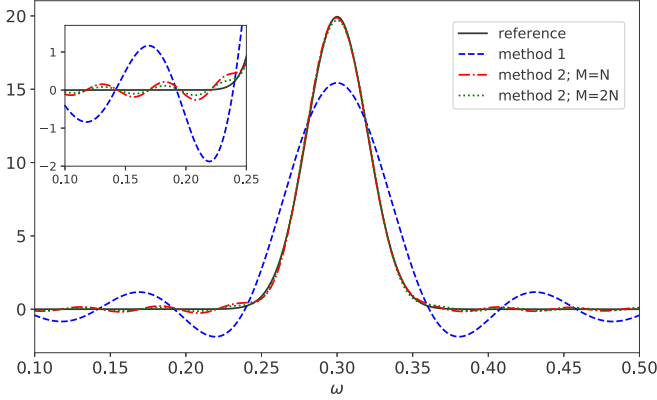
FIG. 8. Reconstruction of the Gaussian signal ($\lambda = 0.05$, $\nu = 0.3$) using two different sets of expansion coefficients given by Eqs. (A17) (*method 1*) and (A20) (*method 2*). In all cases we use $N = 120$ moments. For method 2 we show both $M = 120$ and $M = 240$ integration points.

The coefficients $c_k^{[N,M]}(\nu, \lambda)$ converge close to the exact ones $c_k^{(G)}(\nu, \lambda)$ in the large M limit, and this appears to considerably reduce the truncation error. For the results presented in the main text we use *method 2*, i.e., coefficients of Eq. (A20). To support our choice, in Fig. 8 we present a simple comparison between the two expansions, which shows a faster conversion of *method 2*.

The histogram calculation requires integration over the $c_k^{[N,M]}$ coefficients [see Eq. (32)]. This can be done analytically:

$$
\begin{aligned}
d_k(a, b; \lambda) &= \int_a^b d\nu \, c_k^{[N,M]}(\nu, \lambda) \\
&= \sum_{m=1}^M \frac{\gamma_k}{M} \int_a^b d\nu \, K^{(G)}(\nu, \omega_m; \lambda) T_k(\omega_m) \\
&= \sum_{m=1}^M \frac{\gamma_k}{M} \frac{1}{2} \left[\mathrm{erf}\left(\frac{b - \omega_m}{\sqrt{2}\lambda} \right) - \mathrm{erf}\left(\frac{a - \omega_m}{\sqrt{2}\lambda} \right) \right] T_k(\omega_m).
\end{aligned}
\tag{A21}
$$

APPENDIX B: BOUNDS ON THE TRUNCATION ERROR

In this Appendix we provide the proofs for the bounds on the truncation error β from Eq. (16).

1. Lorentz kernel

Following the derivation in Appendix A 1, for the case of the Lorentzian we have directly a closed-form expression for the expansion coefficients of the integral transform. We can then estimate β by first using

$$
\begin{aligned}
\delta_{trunc}^{(L)} &= \sup_{\nu \in [-1,1]} \left| \sum_{k=N+1}^{\infty} c_k(\nu; \lambda) m_k \right| \\
&\leqslant \sup_{\nu \in [-1,1]} \sum_{k=N+1}^{\infty} |c_k(\nu; \lambda)|,
\end{aligned}
\tag{B1}
$$

and then using the expression for coefficients c_k from Eq. (A5):

$$
\begin{aligned}
\delta_{trunc}^{(L)} &\leqslant \sup_{\nu \in [-1,1]} \frac{2}{\pi \rho} \sum_{n=N+1}^{\infty} e^{-\lambda n} \left| \cos\left[n\left(\nu - \frac{\pi}{2} \right) - \theta \right] \right| \\
&\leqslant \frac{2}{\pi \rho} \sum_{n=N+1}^{\infty} e^{-\lambda n} \\
&\leqslant \frac{2}{\pi \rho} \int_N^{\infty} dx \, e^{-\lambda x} = \frac{2 e^{-\lambda N}}{\lambda \rho \pi}.
\end{aligned}
\tag{B2}
$$

Note at this point that we have also

$$
\rho = [(1 + \nu^2 + \lambda^2)^2 - 4\nu^2]^{1/4} \geqslant \sqrt{1 - \nu^2},
\tag{B3}
$$

but this lower bound is not useful if we keep the spectrum in $[-1, 1]$ as it approaches zero. One option is to rescale the Hamiltonian operator in order to work in a smaller interval, an alternative is to use instead the bound

$$
\rho \geqslant [(2 + \lambda^2)^2 - 4]^{1/4} = \sqrt{\lambda}(4 + \lambda^2)^{1/4} \geqslant \sqrt{2\lambda}.
\tag{B4}
$$

Using this we have the error bound used in the main text:

$$
\beta_N^{(L)} = \frac{\sqrt{2} e^{-\lambda N}}{\lambda^{3/2} \pi}.
\tag{B5}
$$

2. Gaussian kernel

We first compute the bound for the *method 1* approximation in Eq. (A15). First note that we can directly bound the error in the integral transform in terms of the error in the kernel using

$$
\begin{aligned}
&|\Phi(\nu; \lambda) - \Phi_N(\nu; \lambda)| \\
&= \left| \int d\omega \, S(\omega)[K(\nu, \omega; \lambda) - K_N(\nu, \omega; \lambda)] \right| \\
&\leqslant \int d\omega \, S(\omega) |K(\nu, \omega; \lambda) - K_N(\nu, \omega; \lambda)| \\
&\leqslant \sup_{\omega \in [-1,1]} |K(\nu, \omega; \lambda) - K_N(\nu, \omega; \lambda)|,
\end{aligned}
\tag{B6}
$$

where we used that $S(\omega) \geqslant 0$ and normalized to one. Since we perform the exact expansion of the two-variable Chebyshev polynomial $T_k[(\nu - \omega)/2]$ using Eq. (A9) truncated at $m = N \geqslant k$, we find directly that

$$
\begin{aligned}
\delta_{trunc}^{(G),N} &= \sup_{\nu \in [-1,1]} \sup_{\omega \in [-1,1]} |K^{(G)}(\nu, \omega; \lambda) - K^{(G),N}(\nu, \omega; \lambda)| \\
&= \sup_{\nu \in [-1,1]} \sup_{\omega \in [-1,1]} \left| \sum_{k=N+1}^{\infty} a_k\left(\frac{\lambda}{2} \right) T_k\left(\frac{\nu - \omega}{2} \right) \right| \\
&\leqslant \sum_{k=N+1}^{\infty} \left| a_k\left(\frac{\lambda}{2} \right) \right|.
\end{aligned}
\tag{B7}
$$

The sum on the last line was shown in Ref. [39] to be bounded as

$$
\sum_{k=N+1}^{\infty} \left| a_k\left(\frac{\lambda}{2} \right) \right| \leqslant \frac{1}{2\lambda} \sqrt{\frac{\pi}{\kappa(1)}} \mathrm{erfc}\left((N+1)\lambda \sqrt{\frac{\kappa(1)}{2}} \right),
\tag{B8}
$$

where the function κ is given by

$$\kappa(x) = \frac{\log(x + \sqrt{1+x^2})}{2} - \frac{1}{4x}\frac{(x - 1 + \sqrt{1+x^2})^2}{x + \sqrt{1+x^2}}. \quad (B9)$$

Therefore for *method 1* the truncation error can be bounded by

$$\beta_N^{(G)} = \frac{1}{2\lambda}\sqrt{\frac{\pi}{\kappa(1)}}\text{erfc}\left((N+1)\lambda\sqrt{\frac{\kappa(1)}{2}}\right). \quad (B10)$$

For the Gaussian kernel obtained with the *method 2* coefficients from Eq. (A20) we can find a bound on the truncation error (possibly very loose) as follows. First we can use the expansion in Eq. (A8) to reexpress the new expansion coefficients as

$$c_k^{[N,M]}(\nu, \lambda) = \sum_{m=1}^{M}\frac{\gamma_k}{M}\sum_{n=0}^{\infty}a_n\left(\frac{\lambda}{2}\right)T_n\left(\frac{\nu - \omega_m}{2}\right)T_k(\omega_m). \quad (B11)$$

The full kernel can then be written as

$$K^{(G),N,M} = \sum_{k=0}^{N}\sum_{m=1}^{M}\frac{\gamma_k}{M}\sum_{n=0}^{\infty}a_n\left(\frac{\lambda}{2}\right)$$
$$\times T_n\left(\frac{\nu - \omega_m}{2}\right)T_k(\omega_m)T_k(\omega). \quad (B12)$$

At this point it is convenient to define a finite order approximation to the two-variable Chebyshev coefficient as

$$T_n^{N,M}(\nu, \omega) = \sum_{k=0}^{N}\frac{\gamma_k}{M}\sum_{m=1}^{M}T_n\left(\frac{\nu - \omega_m}{2}\right)T_k(\omega_m)T_k(\omega). \quad (B13)$$

Following the discussion used to obtain the Chebyshev coefficients from *method 1*, we know that

$$T_n^{N,M}(\nu, \omega) = T_n\left(\frac{\nu - \omega}{2}\right) \quad \text{for } N \geqslant n, \ M \geqslant n+1. \quad (B14)$$

Using this notation we can write

$$K^{(G),N,M}(\nu, \omega; \lambda) = \sum_{n=0}^{\infty}a_n\left(\frac{\lambda}{2}\right)T_n^{N,M}(\nu, \omega), \quad (B15)$$

while the exact kernel reads

$$K^{(G)}(\nu, \omega; \lambda) = \sum_{n=0}^{\infty}a_n\left(\frac{\lambda}{2}\right)T_n^{n,n+1}\left(\frac{\nu - \omega}{2}\right)$$
$$= \sum_{n=0}^{\infty}a_n\left(\frac{\lambda}{2}\right)T_n\left(\frac{\nu - \omega}{2}\right). \quad (B16)$$

We can then write their difference as

$$K^{(G)}(\nu, \omega; \lambda) - K^{(G),N,M}(\nu, \omega; \lambda)$$
$$= \sum_{n=N+1}^{\infty}a_n\left(\frac{\lambda}{2}\right)\left[T_n\left(\frac{\nu - \omega}{2}\right) - T_n^{N,M}\left(\frac{\nu - \omega}{2}\right)\right], \quad (B17)$$

provided we choose $M \geqslant N+1$.

In order to bound the difference between T_n and $T_n^{N,M}$ defined as

$$\delta_n^N(\nu, \omega) = \left|T_n\left(\frac{\nu - \omega}{2}\right) - T_n^{N,N+1}(\nu, \omega)\right|, \quad (B18)$$

we first recall that, from theorem 2.1 of [55] we have, for any $\omega \in [-1, 1]$, that (see also [52])

$$\delta_n^N(\nu, \omega) \leqslant \left[2 + \frac{2}{\pi}\log(N+1)\right]\left|T_n\left(\frac{\nu - \omega}{2}\right) - p_N^*(\omega)\right|, \quad (B19)$$

where $p_N^*(\omega)$ is the optimal approximating polynomial of order at most N for a given fixed choice of ν (i.e., we look at $T_n[(\nu - \omega)/2]$ as a function of ω only). One option is to now use Jackson's theorems [51] to bound the right-hand side. However, owing to the fact that $n \gg N$ for our purposes, we weren't able to obtain tight bounds in this way. The alternative used to compute the error estimates in the main text was instead to use

$$\left|T_n\left(\frac{\nu - \omega}{2}\right) - p_N^*(\omega)\right| \leqslant \left|T_n\left(\frac{\nu - \omega}{2}\right) - p_0^*(\omega)\right|, \quad (B20)$$

with $p_0^*(\omega)$ the optimal approximating constant. Using the fact that $|T_n(\omega)| \leqslant 1$ together with Corollary 1.6.1 of [51] we have $|T_n[(\nu - \omega)/2] - p_0^*(\omega)| \leqslant 1$ so that

$$\sup_{\nu \in [-1,1]}\sup_{\omega \in [-1,1]}\delta_n^N(\nu, \omega) \leqslant \left[2 + \frac{2}{\pi}\log(N+1)\right]. \quad (B21)$$

In the main text we have then used the following truncation bound for *method 2*

$$\beta_{N,N+1}^{(G)} = \left[2 + \frac{2}{\pi}\log(N+1)\right]\beta_N^{(G)}. \quad (B22)$$

As evident by the results in Fig. 8, where we show a comparison between the kernel function obtained using both methods, this estimate for the truncation error of *method 2* is likely a very conservative upper bound, and we expect in general that $\beta_{N,M}^{(G)} \leqslant \beta_N^{(G)}$. In future work it would be valuable to find tighter error bounds as they will impact the total error budget in the estimation of histograms of the spectral density.

APPENDIX C: ERROR BOUND ON HISTOGRAMS

We want to assess the error for $h(\eta; \Delta)$ defined in Eq. (26). The error has two sources, coming from the fact of using Σ-accurate kernel and from the truncation of the kernel.

Starting from the definition of a histogram of Eq. (27), let us first notice that

$$\widetilde{f}^\Lambda(\eta, \eta; \Lambda) = \int_{\eta-\Lambda}^{\eta+\Lambda}d\nu K(\eta, \nu; \Lambda) \geqslant 1 - \Sigma. \quad (C1)$$

This property also holds for larger intervals $\delta > \Lambda$ and for energies $|\omega - \eta| \leqslant \delta - \Lambda$ as follows:

$$\widetilde{f}^\Lambda(\omega, \eta; \delta) = \int_{\eta-\delta}^{\eta+\delta}d\nu K(\omega, \nu; \Lambda) \geqslant 1 - \Sigma.$$

This is obtained by realizing that $\widetilde{f}^\Lambda(\omega, \eta; \delta)$ is at least $(1 - \Sigma)$ if we can find an interval of size 2Λ, centered in η and contained in the full interval of size 2δ. Since the kernel is normalized, this also implies

$$1 - \widetilde{f}^\Lambda(\omega, \eta; \delta) = \int_{-1}^{\eta-\delta}d\nu K_\Lambda(\omega, \nu) + \int_{\eta+\delta}^{1}d\nu K_\Lambda(\omega, \nu)$$
$$\leqslant \Sigma \quad \text{for} \quad |\omega - \eta| \geqslant \delta + \Lambda. \quad (C2)$$

This condition allows us to construct an approximation of the window function f using its transform. In fact we have the following bound:

$$\sup_{|\omega-\eta|\in[0,\delta-\Lambda]\cup[\delta+\Lambda,\infty]} |f(\omega,\eta;\delta) - \widetilde{f}^{\Lambda}(\omega,\eta;\delta)| \leqslant \Sigma. \quad (C3)$$

The error in the two disjoint intervals has different signs, more explicitly we have

$$\sup_{|\omega-\eta|\in[0,\delta-\Lambda]} [f(\omega,\eta;\delta) - \widetilde{f}^{\Lambda}(\omega,\eta;\delta)] \leqslant \Sigma \quad (C4)$$

since the approximation is always smaller that the indicator function there, and

$$\sup_{|\omega-\eta|\in[\delta+\Lambda,\infty]} [\widetilde{f}^{\Lambda}(\omega,\eta;\delta) - f(\omega,\eta;\delta)]$$

$$= \sup_{|\omega-\eta|\in[\delta+\Lambda,\infty]} \widetilde{f}^{\Lambda}(\omega,\eta;\delta) \leqslant \Sigma. \quad (C5)$$

Let us also notice that

$$f(\omega,\eta;\delta+\Lambda) \geqslant \widetilde{f}^{\Lambda}(\omega,\eta;\delta) \quad \text{for} \quad |\omega-\eta| \leqslant \delta+\Lambda, \quad (C6)$$

Combining Eqs. (C5) and (C6) we find the following lower bound for any ω:

$$f(\omega,\eta;\delta+\Lambda) \geqslant \widetilde{f}^{\Lambda}(\omega,\eta;\delta) - \Sigma. \quad (C7)$$

This immediately implies the following lower bound to the histogram:

$$h(\eta;\Delta) \geqslant \widetilde{h}^{\Lambda}(\eta;\Delta-\Lambda) - \Sigma. \quad (C8)$$

For the upper bound we can use instead

$$f(\omega,\eta;\delta-\Lambda) \leqslant \widetilde{f}^{\Lambda}(\omega,\eta;\delta) \quad \text{for} \quad |\omega-\eta| \geqslant \delta-\Lambda, \quad (C9)$$

together with the (inner) tail condition from Eq. (C4):

$$\widetilde{f}^{\Lambda}(\omega,\eta;\delta) \geqslant 1-\Sigma \quad \text{for} \quad |\omega-\eta| \leqslant \delta-\Lambda. \quad (C10)$$

Combining these two we find the following upper bound for any ω:

$$f(\omega,\eta;\delta-\Lambda) \leqslant \widetilde{f}^{\Lambda}(\omega,\eta;\delta) + \Sigma. \quad (C11)$$

This immediately implies the following lower bound to the histogram:

$$h(\eta;\Delta) \leqslant \widetilde{h}^{\Lambda}(\eta;\Delta+\Lambda) + \Sigma. \quad (C12)$$

The final result is the following two-sided bound on the correct histogram:

$$\widetilde{h}^{\Lambda}(\eta;\Delta-\Lambda) - \Sigma \leqslant h(\eta;\Delta) \leqslant \widetilde{h}^{\Lambda}(\eta;\Delta+\Lambda) + \Sigma. \quad (C13)$$

Including the truncation error, as in Eq. (29), we arrive finally at Eq. (30).

[1] S. Weinberg, Nuclear forces from chiral Lagrangians, Phys. Lett. B **251**, 288 (1990).

[2] S. Weinberg, Effective chiral Lagrangians for nucleon-pion interactions and nuclear forces, Nucl. Phys. B **363**, 3 (1991).

[3] C. Ordóñez, L. Ray, and U. van Kolck, The two nucleon potential from chiral Lagrangians, Phys. Rev. C **53**, 2086 (1996).

[4] D. B. Kaplan, M. J. Savage, and M. B. Wise, Nucleon-nucleon scattering from effective field theory, Nucl. Phys. B **478**, 629 (1996).

[5] E. Epelbaum, W. Gloeckle, and U.-G. Meissner, Low momentum effective theory for nucleons, Phys. Lett. B **439**, 1 (1998).

[6] R. Machleidt and D.R. Entem, Chiral effective field theory and nuclear forces, Phys. Rep. **503**, 1 (2011).

[7] J. D. McDonnell, N. Schunck, D. Higdon, J. Sarich, S. M. Wild, and W. Nazarewicz, Uncertainty Quantification for Nuclear Density Functional Theory and Information Content of New Measurements, Phys. Rev. Lett. **114**, 122501 (2015).

[8] S Wesolowski, N Klco, R J Furnstahl, D R Phillips, and A Thapaliya, Bayesian parameter estimation for effective field theories, J. Phys. G: Nucl. Part. Phys. **43**, 074001 (2016).

[9] J. A. Melendez, S. Wesolowski, and R. J. Furnstahl, Bayesian truncation errors in chiral effective field theory: Nucleon-nucleon observables, Phys. Rev. C **96**, 024003 (2017).

[10] C. Drischler, R. J. Furnstahl, J. A. Melendez, and D. R. Phillips, How Well Do We Know the Neutron-Matter Equation of State at the Densities Inside Neutron Stars? A Bayesian Approach with Correlated Uncertainties, Phys. Rev. Lett. **125**, 202702 (2020).

[11] A. Ekström and G. Hagen, Global Sensitivity Analysis of Bulk Properties of an Atomic Nucleus, Phys. Rev. Lett. **123**, 252501 (2019).

[12] S. König, A. Ekström, K. Hebeler, D. Lee, and A. Schwenk, Eigenvector continuation as an efficient and accurate emulator for uncertainty quantification, Phys. Lett. B **810**, 135814 (2020).

[13] H. Kamada, A. Nogga, W. Glöckle, E. Hiyama, M. Kamimura, K. Varga, Y. Suzuki, M. Viviani, A. Kievsky, S. Rosati *et al.*, Benchmark test calculation of a four-nucleon bound state, Phys. Rev. C **64**, 044001 (2001).

[14] G Orlandini and M Traini, Sum rules for electron-nucleus scattering, Rep. Prog. Phys. **54**, 257 (1991).

[15] J. E. Sobczyk, B. Acharya, S. Bacca, and G. Hagen, Coulomb sum rule for ^{4}He and ^{16}O from coupled-cluster theory, Phys. Rev. C **102**, 064312 (2020).

[16] V. D. Efros, W. Leidemann, and G. Orlandini, Response functions from integral transforms with a Lorentz kernel, Phys. Lett. B **338**, 130 (1994).

[17] V D Efros, W Leidemann, G Orlandini, and N Barnea, The Lorentz integral transform (LIT) method and its applications to perturbation-induced reactions, J. Phys. G: Nucl. Part. Phys. **34**, R459 (2007).

[18] S. Bacca, N. Barnea, G. Hagen, G. Orlandini, and T. Papenbrock, First Principles Description of the Giant Dipole Resonance in ^{16}O, Phys. Rev. Lett. **111**, 122502 (2013).

[19] S. Bacca, N. Barnea, G. Hagen, M. Miorelli, G. Orlandini, and T. Papenbrock, Giant and pigmy dipole resonances in ^{4}He,

^{16,22}O, and ^{40}Ca from chiral nucleon-nucleon interactions, Phys. Rev. C **90**, 064619 (2014).

[20] J. E. Sobczyk, B. Acharya, S. Bacca, and G. Hagen, *Ab Initio* Computation of the Longitudinal Response Function in ^{40}Ca, Phys. Rev. Lett. **127**, 072501 (2021).

[21] J. Carlson and R. Schiavilla, Euclidean Proton Response in Light Nuclei, Phys. Rev. Lett. **68**, 3682 (1992).

[22] J. Carlson, S. Gandolfi, F. Pederiva, S. C. Pieper, R. Schiavilla, K. E. Schmidt, and R. B. Wiringa, Quantum Monte Carlo methods for nuclear physics, Rev. Mod. Phys. **87**, 1067 (2015).

[23] A. Lovato, S. Gandolfi, J. Carlson, S. C. Pieper, and R. Schiavilla, Electromagnetic Response of ^{12}C: A First-Principles Calculation, Phys. Rev. Lett. **117**, 082501 (2016).

[24] M. Jarrell and J.E. Gubernatis, Bayesian inference and the analytic continuation of imaginary-time quantum Monte Carlo data, Phys. Rep. **269**, 133 (1996).

[25] W. Glöckle and M. Schwamb, On the ill-posed character of the Lorentz integral transform, Few-Body Syst. **46**, 55 (2009).

[26] N. Barnea, V. D. Efros, W. Leidemann, and G. Orlandini, The Lorentz integral transform and its inversion, Few-Body Syst. **47**, 201 (2010).

[27] R. N. Silver, D. S. Sivia, and J. E. Gubernatis, Maximum-entropy method for analytic continuation of quantum Monte Carlo data, Phys. Rev. B **41**, 2380 (1990).

[28] E. Vitali, M. Rossi, L. Reatto, and D. E. Galli, *Ab initio* low-energy dynamics of superfluid and solid ^{4}He, Phys. Rev. B **82**, 174510 (2010).

[29] Y. Burnier and A. Rothkopf, Bayesian Approach to Spectral Function Reconstruction for Euclidean Quantum Field Theories, Phys. Rev. Lett. **111**, 182003 (2013).

[30] L. Kades, J. M. Pawlowski, A. Rothkopf, M. Scherzer, J. M. Urban, S. J. Wetzel, N. Wink, and F. P. G. Ziegler, Spectral reconstruction with deep neural networks, Phys. Rev. D **102**, 096001 (2020).

[31] K. Raghavan, P. Balaprakash, A. Lovato, N. Rocco, and S. M. Wild, Machine-learning-based inversion of nuclear responses, Phys. Rev. C **103**, 035502 (2021).

[32] A. Lovato, J. Carlson, S. Gandolfi, N. Rocco, and R. Schiavilla, *Ab initio* study of (ν_ℓ, ℓ^-) and $(\overline{\nu}_\ell, \ell^+)$ inclusive scattering in ^{12}C: Confronting the miniboone and T2K CCQE data, Phys. Rev. X **10**, 031068 (2020).

[33] M. Miorelli, S. Bacca, N. Barnea, G. Hagen, G. R. Jansen, G. Orlandini, and T. Papenbrock, Electric dipole polarizability from first principles calculations, Phys. Rev. C **94**, 034317 (2016).

[34] A. Roggero and S. Reddy, Thermal conductivity and impurity scattering in the accreting neutron star crust, Phys. Rev. C **94**, 015803 (2016).

[35] W. Leidemann, Energy resolution with the Lorentz integral transform, Phys. Rev. C **91**, 054001 (2015).

[36] A. Roggero, F. Pederiva, and G. Orlandini, Dynamical structure functions from quantum Monte Carlo calculations of a proper integral transform, Phys. Rev. B **88**, 094302 (2013).

[37] R. Rota, J. Casulleras, F. Mazzanti, and J. Boronat, Quantum Monte Carlo estimation of complex-time correlations for the study of the ground-state dynamic structure function, J. Chem. Phys. **142**, 114114 (2015).

[38] A. Roggero and J. Carlson, Dynamic linear response quantum algorithm, Phys. Rev. C **100**, 034610 (2019).

[39] A. Roggero, Spectral-density estimation with the Gaussian integral transform, Phys. Rev. A **102**, 022409 (2020).

[40] A. Roggero, A. C. Y. Li, J. Carlson, R. Gupta, and G. N. Perdue, Quantum computing for neutrino-nucleus scattering, Phys. Rev. D **101**, 074038 (2020).

[41] K. Choi, D. Lee, J. Bonitati, Z. Qian, and J. Watkins, Rodeo Algorithm for Quantum Computing, Phys. Rev. Lett. **127**, 040505 (2021).

[42] R. D Somma, Quantum eigenvalue estimation via time series analysis, New J. Phys. **21**, 123025 (2019).

[43] P. Rall, Quantum algorithms for estimating physical quantities using block encodings, Phys. Rev. A **102**, 022408 (2020).

[44] M. Carmen Bañuls, R. Blatt, J. Catani, A. Celi, J. Ignacio Cirac, M. Dalmonte, L. Fallani, K. Jansen, M. Lewenstein, S. Montangero *et al.*, Simulating lattice gauge theories within quantum technologies, Eur. Phys. J. D **74**, 165 (2020).

[45] N. Klco, A. Roggero, and M. J. Savage, Standard model physics and the digital quantum revolution: Thoughts about the interface, arXiv:2107.04769.

[46] A. Weiße, G. Wellein, A. Alvermann, and H. Fehske, The kernel polynomial method, Rev. Mod. Phys. **78**, 275 (2006).

[47] F. Alexander Wolf, I. P. McCulloch, O. Parcollet, and U. Schollwöck, Chebyshev matrix product state impurity solver for dynamical mean-field theory, Phys. Rev. B **90**, 115124 (2014).

[48] Y. Yang, S. Iblisdir, J. Ignacio Cirac, and M. Carmen Bañuls, Probing Thermalization through Spectral Analysis with Matrix Product Operators, Phys. Rev. Lett. **124**, 100602 (2020).

[49] I. Papaefstathiou, D. Robaina, J. Ignacio Cirac, and M. Carmen Bañuls, Density of states of the lattice Schwinger model, Phys. Rev. D **104**, 014514 (2021).

[50] D. Jackson, On approximation by trigonometric sums and polynomials, Trans. Am. Math. Soc. **13**, 491 (1912).

[51] T.J. Rivlin, *An Introduction to the Approximation of Functions*, Blaisdell Books in Numerical Analysis and Computer Science (Dover Publications, New York, 1981).

[52] R. Günttner, Evaluation of Lebesgue constants, SIAM J. Numer. Anal. **17**, 512 (1980).

[53] D. Moldovan, M. Anđelković, and F. Peeters, pybinding v0.9.5: A Python package for tight-binding calculations (2020)10.5281/zenodo.826942.

[54] A. Vijay, D. J. Kouri, and D. K. Hoffman, Scattering and bound states: A Lorentzian function-based spectral filter approach, J. Phys. Chem. A **108**, 8987 (2004).

[55] Z. Battles and L. N. Trefethen, An extension of MATLAB to continuous functions and operators, SIAM J. Sci. Comput. **25**, 1743 (2004).